Society For Biomaterials

Graphene oxide nanoparticles for enhanced photothermal cancer cell therapy under the irradiation of a femtosecond laser beam

Jing-Liang Li,[1] Xue-Liang Hou,[1] Hong-Chun Bao,[2] Lu Sun,[1] Bin Tang,[1] Jin-Feng Wang,[1] Xun-Gai Wang,[1] Min Gu[2]

[1]Institute for Frontier Materials, Deakin University, Waurn Ponds, Victoria 3216, Australia
[2]Faculty of Engineering and Industrial Science, Centre for Micro-Photonics, Swinburne University of Technology, Hawthorn, Victoria 3122, Australia

Received 7 May 2013; revised 24 June 2013; accepted 27 June 2013
Published online 10 August 2013 in Wiley Online Library (wileyonlinelibrary.com). DOI: 10.1002/jbm.a.34871

Abstract: Nano-sized graphene and graphene oxide (GO) are promising for biomedical applications, such as drug delivery and photothermal therapy of cancer. It is observed in this work that the ultrafast reduction of GO nanoparticles (GONs) with a femtosecond laser beam creates extensive microbubbling. To understand the surface chemistry of GONs on the microbubble formation, the GONs were reduced to remove most of the oxygen-containing groups to get reduced GONs (rGONs). Microbubbling was not observed when the rGONs were irradiated by the laser. The instant collapse of the microbubbles may produce microcavitation effect that brings about localized mechanical damage. To understand the potential applications of this phenomenon, cancer cells labeled with GONs or rGONs were irradiated with the laser. Interestingly, the microbubbling effect greatly facilitated the destruction of cancer cells. When microbubbles were produced, the effective laser power was reduced to less than half of what is needed when microbubbling is absent. This finding will contribute to the safe application of femtosecond laser in the medical area by taking advantage of the ultrafast reduction of GONs. It may also find other important applications that need highly localized microcavitation effects. © 2013 Wiley Periodicals, Inc. J Biomed Mater Res Part A: 102A: 2181–2188, 2014.

Key Words: graphene oxide, reduced graphene oxide, femtosecond laser, microcavitation, photothermal treatment

How to cite this article: Li J-L, Hou X-L, Bao H-C, Sun L, Tang B, Wang J-F, Wang X-G, Gu M. 2014. Graphene oxide nanoparticles for enhanced photothermal cancer cell therapy under the irradiation of a femtosecond laser beam. J Biomed Mater Res Part A 2014:102A:2181–2188.

INTRODUCTION

Graphene has excellent mechanical and physical properties.[1,2] Besides the general interest in electronic applications of graphene, graphene and its derivatives are promising materials for biomedical applications.[3] In this regard, graphene oxide (GO) is a subject of particular interest due to its richness in functional groups. This facilitates its surface functionalization for applications such as drug delivery,[4,5] biosensing, and bioimaging.[6–10] Recently, there has been a growing interest in using graphene-related nanomaterials for photothermal therapy of cancer and other diseases.[3,8,11–13] Due to its high light absorption, reduced GO has been of particular interest when a continuous wave laser is used.[14,15] Temperature increase in the nanoparticles caused by laser irradiation is the mechanism of cell therapy.

The production of graphene largely relies on the reduction of its oxidized form (i.e., GO) in water. The general methods to reduce GO include chemical[16,17] and physical (heat and light exposure) approaches.[18,19] With the physical methods, the oxygen-containing groups such as carboxylic and hydroxyl groups on GO can be removed with the release of gases such as CO_2 and H_2O. As a physical tool, laser has been used to reduce GO, leading to precise micromachining of electronic devices.[18] Ultrafast laser is an effective tool for nanofabrication due to the high pulse energy.[20,21] Under the irradiation of such a laser, the temperature of graphene can be increased to a few thousand degrees in microseconds.[8,22] The ultrafast temperature increase can in principle reduce GO simultaneously. This in turn will lead to simultaneous release of gases, promoting instant formation and collapse of microbubbles in a solution. The high pressure caused by the collapse of microbubbles (microcavitation) has many important applications such as micro/nanovoids formation for fabrication of photonic crystals and cancer cell therapy. In our recent article, microbubbling from graphene oxide nanoparticles (GONs) under the irradiation of a femtosecond laser beam has been observed and the collapse of microbubbles was accompanied with the damage of cancer cells.[8] However, the mechanism of microbubbling and the contribution of microcavitation to cancer cell therapy were not understood. A good understanding of these is essential to the design of an energy efficient photothermal treatment.

Additional Supporting Information may be found in the online version of this article.
Correspondence to: X.-G. Wang; e-mail: xwang@deakin.edu.au or M. Gu; e-mail: mgu@swin.edu.au

In this work, the microbubble formation enhanced by GONs under the irradiation of a femtosecond laser beam and its effects on *in vitro* cancer cell damage were examined. GONs were prepared using a modified Hummers method.[23] Reduced GONs (rGONs) were obtained by ultraviolet (UV) irradiating GONs to remove most of the oxygen-containing groups from the surface of the nanoparticles. It is anticipated that microbubbling can be suppressed if most of the functional groups are removed. Hence, the contribution of microcavitation to cell therapy can be elucidated by comparing the efficiency of GONs and rGONs. Interestingly, it was observed that under the irradiation of a femtosecond laser beam, extensive microbubbling could be produced from GONs in aqueous medium. The production of microbubbles and their collapse occurred in microseconds. Microbubbling was not observed in the case of rGONs. The microcavitation induced by the ultrafast reduction of GONs lowered the effective laser power for therapy from 9 mW to 4 mW.

MATERIALS AND METHODS

Materials

Graphite, Transferrin, fetal bovine serium, Roswell Park Memorial Institute medium-1640 medium containing L-glutamine and sodium bicarbonate, calcein acetoxymethyl (AM), ethidium bromide, and phosphate-buffered saline (PBS) tablets were obtained from Sigma. Amine-functionalized polyethylene glycol (PEG-NH_2, MW 5000) was obtained from Nanocs. All the chemicals were used as received.

Preparation and characterization of GONs

GO was obtained by exfoliating graphite following a reported method with modifications.[23] The GO solution was then sonicated for 30 min to yield a mixture of particles and sheets. GONs were harvested by centrifuging the solution of the mixture at 25,000 rcf for 30 min to remove the GO sheets.

Reduction of GONs

To obtain rGONs, 40 mL of GONs at a concentration of 50 μg/mL was contained in a sample weighting plate and subjected to UVB irradiation for 24 h. After irradiation, the final volume was adjusted to 40 mL. The UV–visible absorption of the particle solutions was measured.

X-Ray photoelectron spectroscopy

X-ray photoelectron spectroscopy was used to characterize the surface functional groups of GONs after light irradiation. A monochromatized X-ray source (He I, $h\nu$ =21.2 eV) was used.

Surface functionalization of GONs and rGONs

To coat GONs and rGONs with transferrin molecules, aliquots of concentrated transferrin was added into 10 mL of GONs (50 μg/mL) or rGONs (50 μg/mL) dispersion in water. The transferrin-coated nanoparticles were centrifuged to remove excess transferrin molecules and dispersed in cell culture medium RMPI for *in vitro* therapy. The concentration of transferrin molecules on nanoparticles was calculated from the transferrin concentrations in the initial solution and in the supernatant after conjugation, as measured by a UV–visible spectrometer. By tuning the concentration of transferrin, the ratio of transferrin to nanoparticles was achieved the same (0.25:1 by weight) for GONs and rGONs. To stabilize the nanoparticles in culture buffer, PEG-NH_2 (molecular weight 5000) was also coated on the nanoparticles after protein coating. The excessive PEG-NH_2 was removed by centrifuging the nanoparticles and redisperse them in PBS buffer.

Microbubbling testing on glass cover slips

An Olympus Fluoview inverted scanning microscope (FV300) was used for microbubbling examination on cover slips and for treatment of cancer cells. The laser is a femotosecond Ti:sapphire laser (MaiTai, Spectra Physics) with a repetition rate of 80 MHz, a pulse width of 100 fs and a tunable wavelength from 690 nm to 1040 nm. The wavelength was fixed at 800 nm. A water immersion objective lens (60×, NA: 1.2) was used. A small volume of dilute dispersion of GONs or rGONs was deposited on a cover slip. The sample was dried naturally at room temperature. Before imaging, a small drop of water was put on each cover slip to cover the nanoparticles.

In vitro therapy

To evaluate the microcavitation effect on cancer cell therapy, a gastric cancer cell line (AGS) was used as a model. The cancer cells were labeled with either transferrin-coated GONs or transferrin-coated rGONs. Cells were incubated with nanoparticles for 6 h in 24-well plates with cover slips as bottom of the wells. When cells had been incubated with the nanoparticles for 5.5 h, 10 μL of concentrated calcein AM was added into each well. The concentration of calcein AM in the cell culture medium was 10 μ*M*. After 30 min, the cells were washed twice with PBS and fresh medium (0.5 mL) was then added into each well. The incident power was measured at the focus point. After treatment, the laser power was reduced to 3 mW to avoid further cell damage during imaging.

RESULTS AND DISCUSSION

GO prepared in this work is a mixture of micrometer-sized large sheets and small GONs (Supporting Information Fig. S1; the fraction of GONs by weight is about 25%). GONs were harvested with a centrifuge. An AFM image of the GONs is shown in Figure 1(a). Dynamic laser scattering indicates that the size of the nanoparticles is peaked at 28 nm [Fig. 1(b)]. A three-dimensional (3D) AFM measurement shows that the thickness of GONs ranges from a few nanometers to 12.5 nm. This indicates the nanoparticles consist of multilayers of graphene. To get rGONs, a dilute dispersion of GONs in water was irradiated with a UV light (UVB) for 24 h. Further irradiation led to aggregation of the nanoparticles, meaning that most of the hydrophilic groups on the

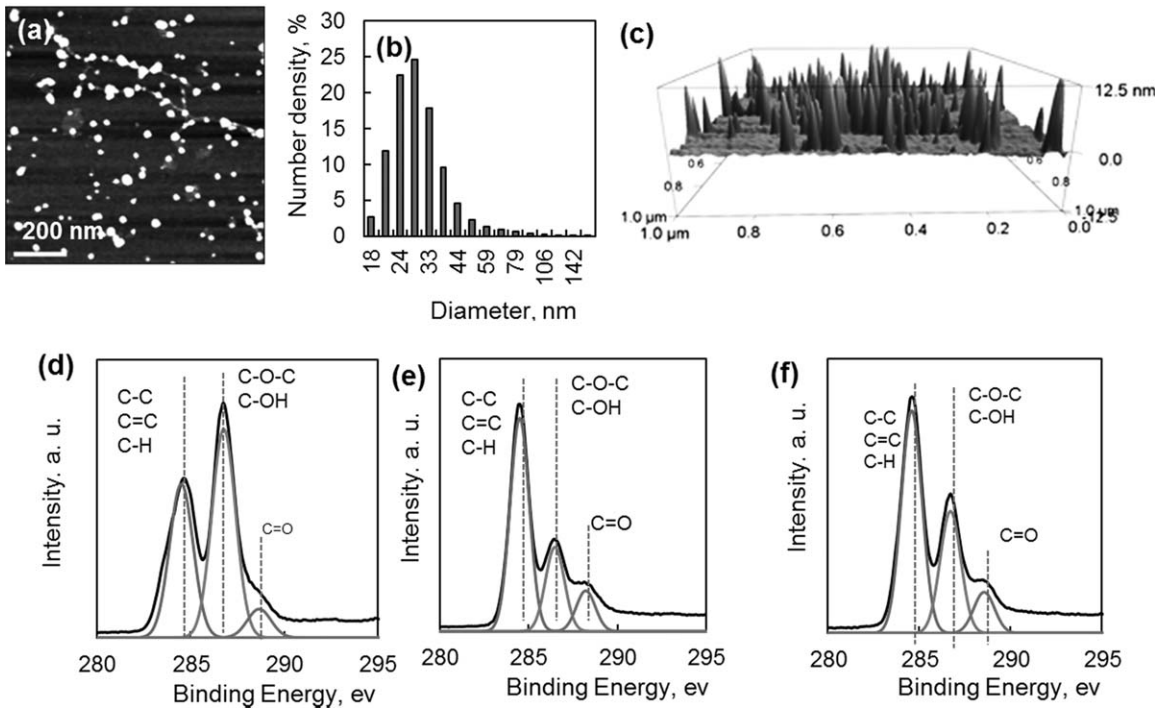

FIGURE 1. Characterization of GONs and rGONs. (a) AFM images of as-synthesized GONs, (b) particle size distribution from dynamic light scattering, (c) a 3D images of GONs, XPS spectra of (d) GONs, (e) rGONs, and (f) GONs after being scanned with a femtosecond laser beam three times at 8 mW. The results in (d) and (e) show that most of the oxygen-containing groups particularly the hydroxyl groups (C–OH) and epoxy groups (C–O–C) have been removed in the rGONs.

surface of the nanoparticles were removed, which is also proven by the surface characterization with XPS.

The microbubbling of water, in the presence of GONs and rGONs when excited by a femtosecond laser beam, was examined on glass cover slips. This experiment and those for cell therapy were performed on an Olympus Fluoview-300. The laser is from Spectra Physics, with a repetition rate of 80 MHz and a pulse width of 100 fs. The wavelength was fixed at 800 nm. For GONs, it was observed that extensive microbubbling occurred when the laser power was above 4 mW. This was not observed in the case of rGONs, due to the presence of minimal oxygen-containing groups on these nanoparticles. Nano-sized graphene and GO have demonstrated strong two-photon luminescence (TPL), which enables their imaging both *in vitro* and *in vivo*.[8,24–26] Figure 2 gives both the TPL images and transmission images of GONs and rGONSs after being raster scanned at 8 mW. It was also observed that the number of microbubbles reduced quickly, with most of them disappeared after three scans, indicating the fast reduction of GONs. The scanning area was fixed at 80 μm × 80 μm and each scan took one second. On the basis of these, it is estimated that the exposure time of one nanoparticle to laser in one raster scan is about 20 μs.[27] This means that the reduction of GONs takes place quickly within microseconds. Such a fast reduction is attributable to the high peak power of a laser pulse. For a pulsed laser with a repetition rate of 80 MHz and a pulse width of 80 fs, the pulse peak power is 1.25 kW at an average laser power of 8 mW. In addition, the instant high temperature increase also contributes to the ultrafast thermal reduction of GONs. XPS characterization indicates that about half of the oxygen-containing groups [as compared to Fig. 1(d)] was removed after three scans at this laser power [Fig. 1(f)].

To illustrate the potential applications of the ultrafast reduction of GO, the effects of microbubbling on cancer cell therapy was performed *in vitro*. A gastric cancer cell line (AGS) was used as a model. To facilitate cellular uptake of the nanoparticles and to stabilize the nanoparticles in cell culture buffer, both the GONs and rGONs were coated with transferrin molecules and PEG molecules physically. The selection of a physical other than a covalent conjugation method is based on the consideration that GONs and rGONs have different contents of functional groups. This will make it hard to functionalize them with a same amount of protein molecules. Graphene has an excellent affinity to protein and PEG. Physically coating is generally used for the functionalization of rGONs.[28] Transferrin has been proven to be an effective ligand for targeting various cancer cells due to the upregulation of transferrin receptors on cancer cells.[27,29–32] The number of transferrin molecules adsorbed on GONs and rGONs were kept the same by adjusting the concentration of transferrin. Each milligram of GONs or rGONs was coated with 0.25 mg of transferrin. UV–visible absorption indicates the coating of transferrin on the nanoparticles (Fig. 3).

TPL imaging indicates that the cellular uptake of GONs and rGONs is similar (Fig. 4). When the particles are not coated with transferrin, significantly reduced cellular

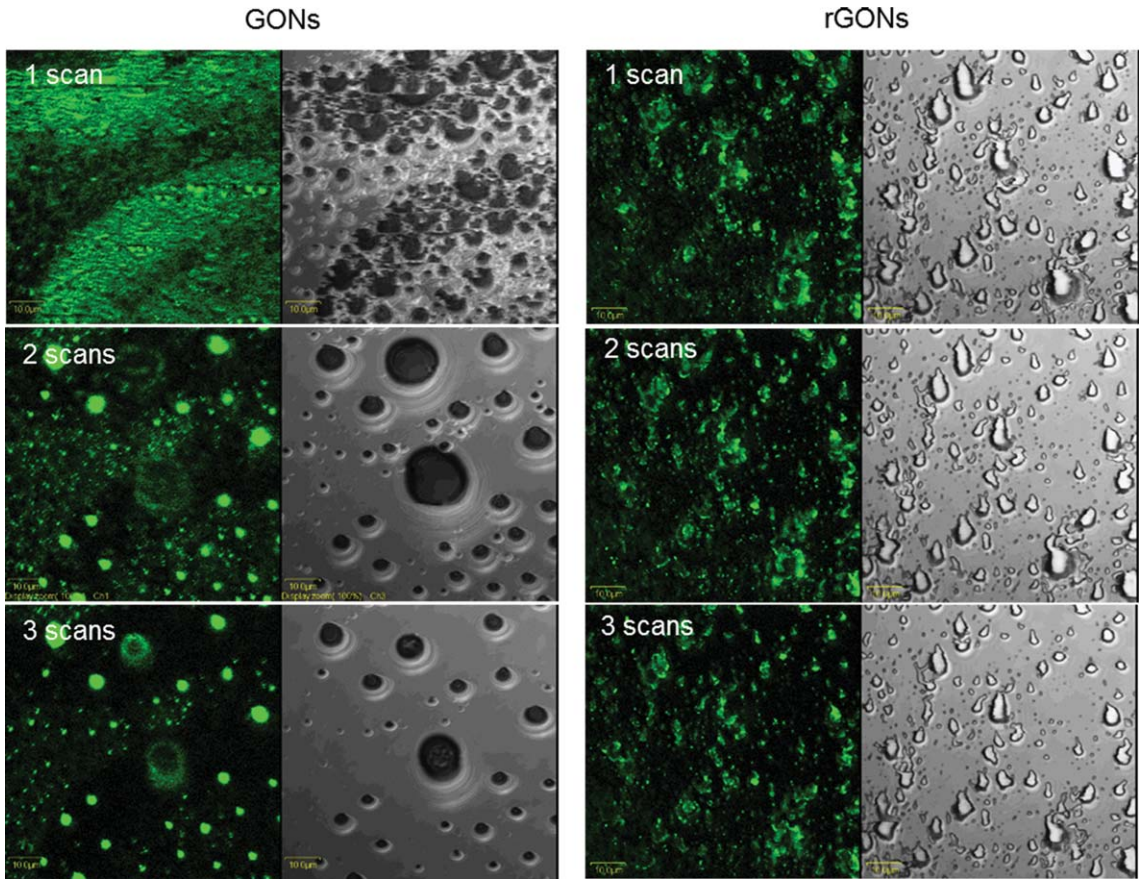

FIGURE 2. Examination of microbubble formation from GONs and rGONs deposited on cover slips. The laser power was fixed at 8 mW. The scale bars represent 10 μm. [Color figure can be viewed in the online issue, which is available at wileyonlinelibrary.com.]

targeting of both GONs and rGONs was observed. The concentrations of the particles were fixed at 50 μg/mL. No toxicity to cells was observed for both types of nanoparticles at this concentration. Good *in vitro* and *in vivo* biocompatibility of GO and reduced GO has also been reported.[8,15,33] For *in vitro* work, the nanoparticles at concentrations up to more than 200 μg/mL did not show obvious toxicity to cells. For *in vivo* work, GO nanosheets at a dose of 20 mg/kg did not show any toxicity to mice.[33] In this work, the cells were incubated with the nanoparticles for 6 h before imaging was taken. Therefore, the images show that most of the nanoparticles were localized on the membrane of cells. For chemotherapy, delivery of drug carrier nanoparticles into cells is necessary for efficient treatment. In contrast, photothermal treatment aims to destroy cells physically, which makes it not necessary to deliver nanoparticles into cells. It has been demonstrated that more efficient photothermal treatment can be achieved when gold nanorods were attached to cell membrane since cell membrane is more liable to thermal shock.[34]

Figure 5 gives the images of *in vitro* cell therapy using the femtosecond laser. Calcein AM was used to examine the effects of laser irradiation on cell viability. Calcein AM is a nonfluorescent hydrophobic dye that can enter live and intact cells easily. A live cell emits green fluorescence and the color fades when the viability of a cell is compromised. It was observed that when cells were not labeled with particles (row 1, Fig. 5), a high laser power had to be used to bring about therapeutic effects. After cells were raster scanned 45 times at a laser power of 25 mW, the viability of a fraction of cells in the irradiated area diminished, which was accompanied with extensive membrane blebbing (the left two images in row 1). Membrane blebbing often occurs when a cell is under stresses such as the presence of toxins and introduction of a thermal shock.[27,34] When the laser power was increased to 30 mW, instant damage to cell membrane was observed (the right two images in row 1). Interestingly, when cells were labeled with GONs, a few scans at a power above 4 mW were enough for cell therapy (row 2, Fig. 5). The fluorescence from calcein AM in some cells disappeared during the raster scanning, indicating the instant damage of cells by the nanoparticles. When cells were labeled with rGONs, significant reduction in cell viability was achieved when the cells were scanned 15 times at a laser power of 9 mW, while only a small fraction of cells were dead after the cells were scanned a hundred times at 8 mW. This is in sharp contrast to the cells labeled with GONs. In that case, a few raster scans are enough to induce cell death at this laser power. Considering the similar cellular uptakes of the nanoparticles, the difference should be

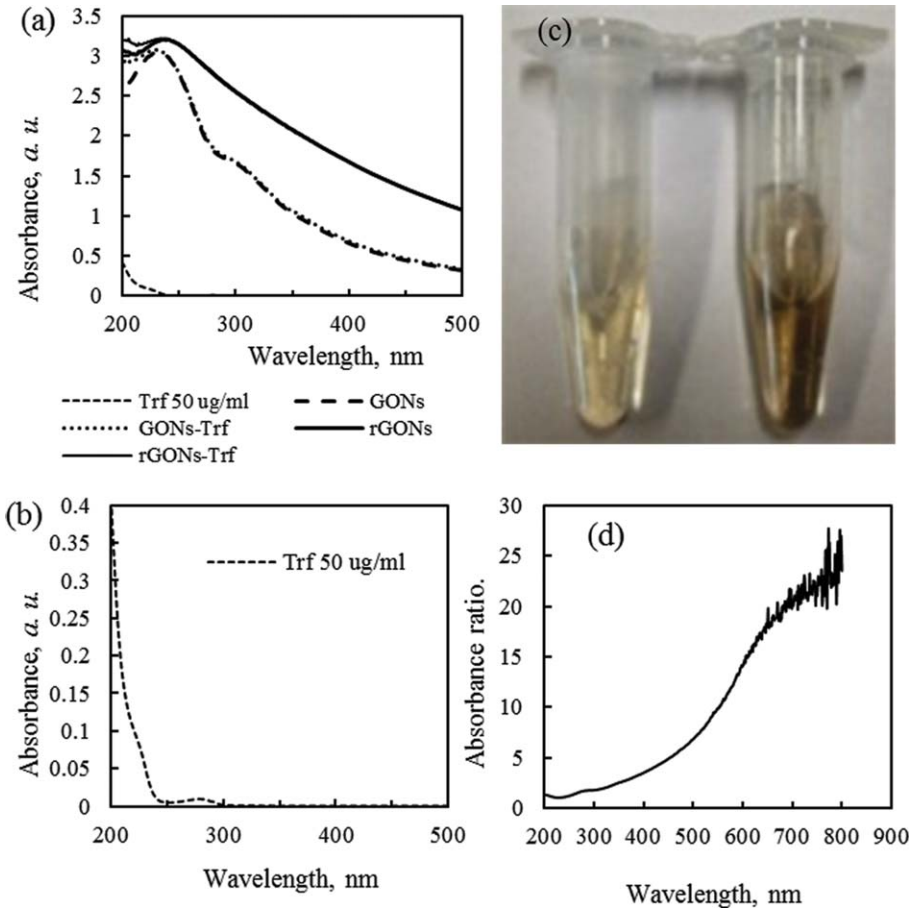

FIGURE 3. (a) UV–visible absorption spectra of GONs, GON-Trf, rGONs, and rGO-Trf and free transferrin (Trf) molecules in PBS buffer, (b) is enlarged from (a) to show the absorption peak of transferrin at 280 nm. Due to the low concentration of Trf, the characteristic absorption peak at 280 nm is not obvious on the Trf-coated GONs (GONs-Trf) and Trf-coated rGONs(rGONs-Trf). However, the presence of Trf is evidenced by the absorbance change in the wavelength between 200 nm and 250 nm, (c) an optical image of the GONs and rGONs dispersed in water (left: GONs; right: rGONs), and (d) absorbance ratio of rGONs to GONs at different wavelengths. With increase in wavelength, the ratio increases and approaches a constant. The absorbance of rGONs is a magnitude higher than that of GONs at a wavelength above 550 nm (ratio is larger than 10). The concentration of both GONs and rGONs is 50 μg/mL. [Color figure can be viewed in the online issue, which is available at wileyonlinelibrary.com.]

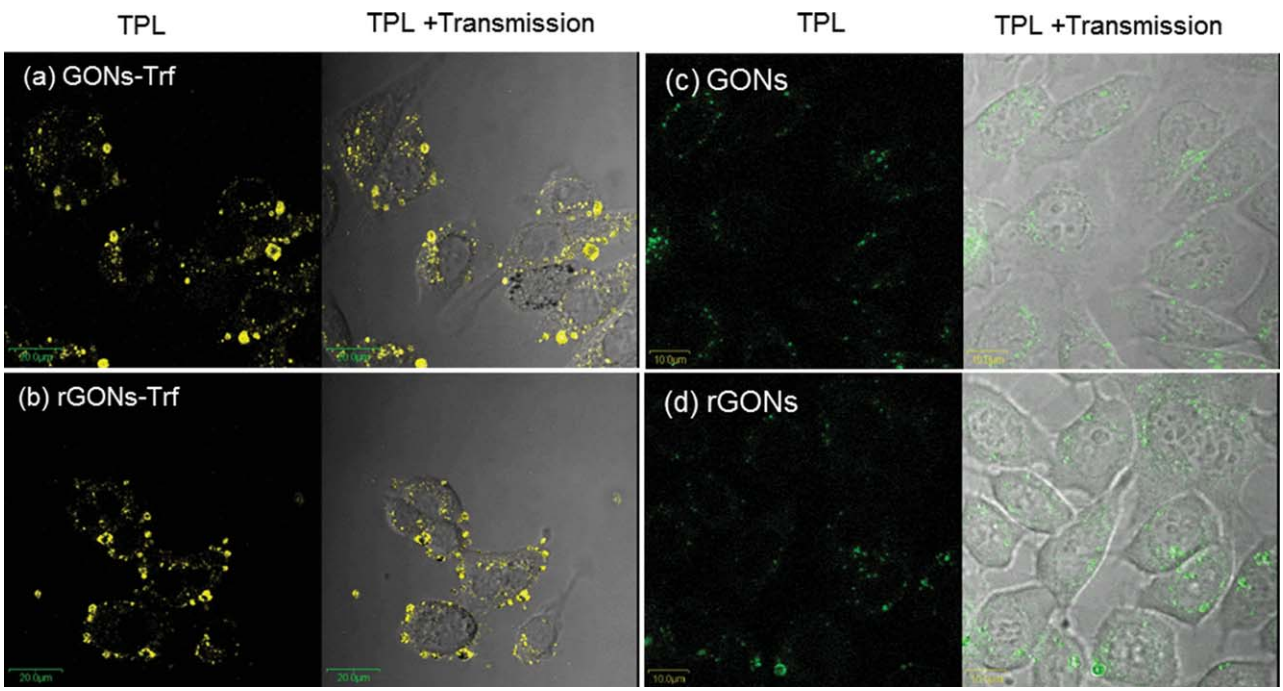

FIGURE 4. *In vitro* two-photon luminescence (TPL) imaging of (a) transferrin-coated GONs (GONs-Trf), (b) transferrin-coated rGONs (rGONs-Trf), and not functionalized (c) GONs and (d) rGONs. Gastric (AGS) cancer cells were used. [Color figure can be viewed in the online issue, which is available at wileyonlinelibrary.com.]

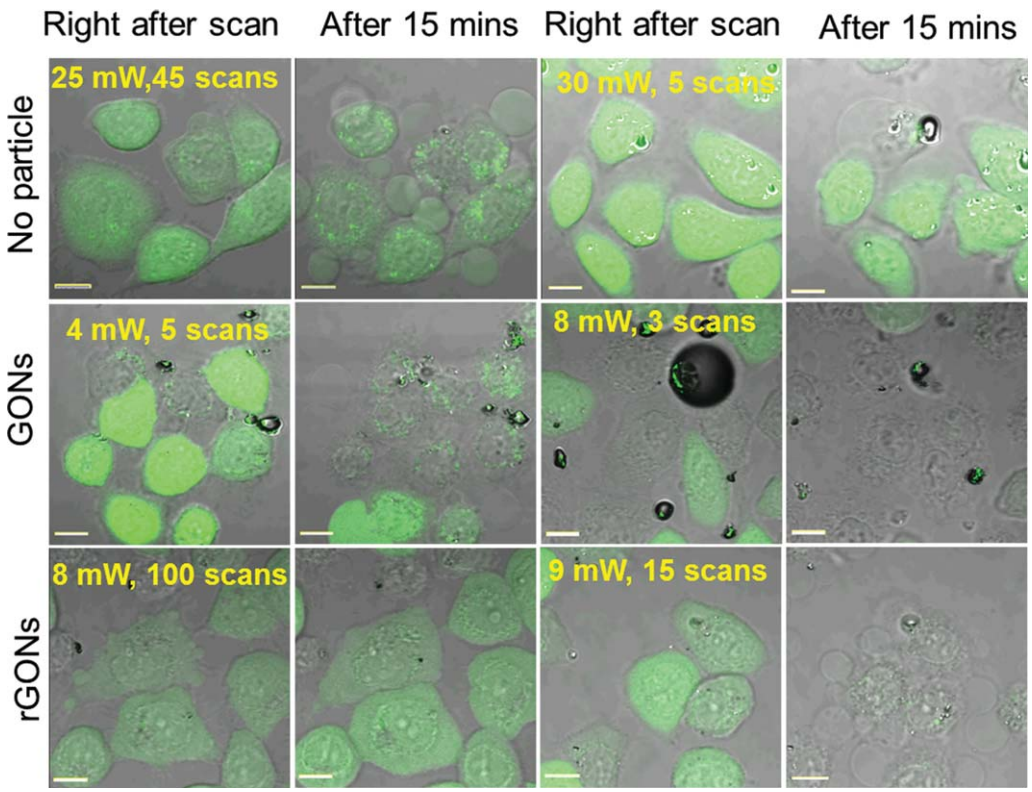

FIGURE 5. Laser therapy of cells without nanoparticle labeling (row 1), labeled with GONs (row 2), and (c) rGONs (row 3). To avoid further damage to cells, the laser power was reduced to 3 mW for imaging. The GONs and rGONs are functionalized with transferrin to enhance their cellular uptake. All the images were taken at a same photomultiplier (PMT) level (700). The scale bars represent 10 μm. [Color figure can be viewed in the online issue, which is available at wileyonlinelibrary.com.]

caused by the microbubble formation. When cells were labeled with GONs, the collapse of microbubbles can create a high mechanical force which compromises the cell membrane instantly. Unlike the case of GONs, microbubbling was not observed for cells labeled with rGONs. Instead, extensive cell membrane blebbing was observed (the right most image of row 3), which is similar to what happened to cells without nanoparticle labeling (25 mW, 45 scans). This means that the in these two cases, the cell death should be caused by the photothermal effects similarly. The numbers of scan need to bring about cell death are summarized in Figure 6. When cells were not labeled with particles, cell death was not observed after they were raster scanned 200 times. The different effects of GONs and rGONs on photothermal therapy were also demonstrated for noncancerous skin cells (HFF; Supporting Information Fig. S2). Due to the lower uptake of the nanoparticles by HFF cells, a power of 11 mW (five raster scans) was observed to induce therapeutic effects on cells labeled with GONs. In contrast, no cell damage were observed when the laser power was increased to 15 mW (50 raster scans) when the cells were labeled with rGONs.

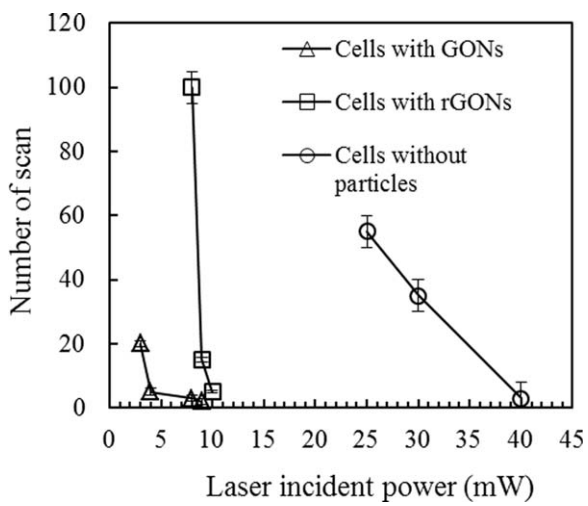

FIGURE 6. Numbers of laser raster scan needed to bring about cell death.

Due to its high light absorption, reduced GO has been a preferable choice for photothermal treatment when continuous wave lasers were used.[14,35,36] As is shown by the UV-visible absorption spectra [Fig. 3(a)], the rGONs have much higher light absorption than GONs. This is also indicated by the optical images of the dispersions of the particles in water [Fig. 3(c)]. At a wavelength of 800 nm, which was used for cancer cell treatment in this work, the absorbance of rGONs is more than twenty times of that of GONs [Fig. 3(d)]. Considering the sizes of the nanoparticles are much

smaller than the wavelength of the incident laser, the energy loss due to scattering is negligible. Therefore, the energy absorbed by rGONs is more than 20 times of that by GONs, which means that the temperature rise of rGONs should be higher than GONs. If only temperature increase contributes to cell death, rGONs should be more effective than GONs. The fact that GONs are more effective than rGONs indicates the microcavitation effect contributes more to cell therapy.

CONCLUSIONS

In summary, it is demonstrated that the ultrafast reduction of GO can promote microbubbling of water that helps to destruct cancer cells. The *in vitro* testing in this study showed that the microbubbles were produced only on cells labeled with GONs and the microbubbles collapsed instantly, so hopefully they may not disturb the local blood flow in an *in vivo* situation. More importantly, near infrared pulsed laser is the light source for multiphoton microscopy, which has been used as a tool for deep tissue imaging and cell therapy.[37,38] With the imaging capability of multi-photon microscopy, the laser exposure can be precisely controlled on the malignant cells. Low and high intensity lasers can be used to image/identify and treat malignant cells, respectively. In this way, hazard to adjacent normal cells and blood vessels can be prevented. The observations in this work indicate that by combining multiphoton microscopy (powered by a femtosecond laser) and GONs, low energy and *in vivo* laser microsurgery of cancer is achievable. More detailed and in-depth work including long term monitoring of the photothermal effects on cells after treatment and *in vivo* therapy are interesting for further research. The microcavitation effect caused by the instant physical–chemical changes in GO can be hopefully used for the applications beyond cancer treatment such as voids creation for fabrication of photonic crystals.

REFERENCES

1. Li D, Mueller MB, Gilje S, Kaner RB, Wallace GG. Processable aqueous dispersions of graphene nanosheets. Nat Nanotechnol 2008;3:101–105.
2. Geim AK. Graphene: Status and prospects. Science 2009;324: 1530–1534.
3. Yang K, Feng L, Shi X, Liu Z. Nano-graphene in biomedicine: Theranostic applications. Chem Soc Rev 2013;42:530–547.
4. Yang X, Zhang X, Liu Z, Ma Y, Huang Y, Chen Y. High-efficiency loading and controlled release of doxorubicin hydrochloride on graphene oxide. J Phys Chem C 2008;112:17554–17558.
5. Pan Y, Sahoo NG, Li L. The application of graphene oxide in drug delivery. Expert Opin Drug Del 2012;9:1365–1376.
6. Chen JL, Yan XP, Meng K, Wang SF. Graphene oxide based photoinduced charge transfer label-free near-infrared fluorescent biosensor for dopamine. Anal Chem 2011;83:8787–8793.
7. Luo M, Chen X, Zhou G, Xiang X, Chen L, Ji X, He Z. Chemiluminescence biosensors for DNA detection using graphene oxide and a horseradish peroxidase-mimicking DNAzyme. Chem Commun 2012;48:1126–1128.
8. Li JL, Bao HC, Hou XL, Su L, Wang XG, Gu M. Graphene oxide nanoparticles as a nonbleaching optical probe for two-photon luminescence imaging and cell therapy. Angew Chem Int Ed Engl 2012;51:1830–1834.
9. He S, Liu K-K, Su S, Yan J, Mao X, Wang D, He Y, Li L, Song S, Fan C. Graphene-based high-efficiency surface-enhanced Raman scattering-active platform for sensitive and multiplex DNA detection. Anal Chem 2012;84:4622–4627.
10. Pei H, Li J, Lv M, Wang J, Gao J, Lu J, Li Y, Huang Q, Hu J, Fan C. A graphene-based sensor array for high-precision and adaptive target identification with ensemble aptamers. J Am Chem Soc 2012;134:13843–13849.
11. Markovic ZM, Harhaji-Trajkovic LM, Todorovic-Markovic BM, Kepic DP, Arsikin KM, Jovanovic SP, Pantovic AC, Dramicanin MD, Trajkovic VS. In vitro comparison of the photothermal anticancer activity of graphene nanoparticles and carbon nanotubes. Biomaterials 2011;32:1121–1129.
12. Li M, Yang X, Ren J, Qu K, Qu X. Using graphene oxide high near-infrared absorbance for photothermal treatment of Alzheimer's disease. Adv Mater 2012;24:1722–1728.
13. Shi X, Gong H, Li Y, Wang C, Cheng L, Liu Z. Graphene-based magnetic plasmonic nanocomposite for dual bioimaging and photothermal therapy. Biomaterials 2013;34: 4786–4793.
14. Yang K, Hu LL, Ma XX, Ye SQ, Cheng L, Shi XZ, Li CH, Li YG, Liu Z. Multimodal imaging guided photothermal therapy using functionalized graphene nanosheets anchored with magnetic nanoparticles. Adv Mater 2012;24:1868–1872.
15. Yang K, Wan J, Zhang S, Tian B, Zhang Y, Liu Z. The influence of surface chemistry and size of nanoscale graphene oxide on photothermal therapy of cancer using ultra-low laser power. Biomaterials 2012;33:2206–2214.
16. Stankovich S, Dikin DA, Piner RD, Kohlhaas KA, Kleinhammes A, Jia Y, Wu Y, Nguyen ST, Ruoff RS. Synthesis of graphene-based nanosheets via chemical reduction of exfoliated graphite oxide. Carbon 2007;45:1558–1565.
17. Wang G, Yang J, Park J, Gou X, Wang B, Liu H, Yao J. Facile synthesis and characterization of graphene nanosheets. J Phys Chem C 2008;112:8192–8195.
18. Gao W, Singh N, Song L, Liu Z, Reddy ALM, Ci L, Vajtai R, Zhang Q, Wei B, Ajayan PM. Direct laser writing of micro-supercapacitors on hydrated graphite oxide films. Nat Nanotechnol 2011;6:496–500.
19. Zhang Y, Guo L, Wei S, He Y, Xia H, Chen Q, Sun H, Xiao F. Direct imprinting of microcircuits on graphene oxides film by femtosecond laser reduction. Nano Today 2010;5:15–20.
20. Choi K, Zijlstra P, Chon JWM, Gu M. Fabrication of low-threshold 3d void structures inside a polymer matrix doped with gold nanorods. Adv Funct Mater 2008;18:2237–2245.
21. Zhang Q, Lin H, Jia B, Xu L, Gu M. Nanogratings and nanoholes fabricated by direct femtosecond laser writing in chalcogenide glasses. Opt Express 2010;18:6885–6890.
22. Yang H, Feng X, Wang Q, Huang H, Chen W, Wee ATS, Ji W. Giant two-photon absorption in bilayer graphene. Nano Lett 2011; 11:2622–2627.
23. Hummers WS, Offeman RE. Preparation of graphene oxide. J Am Chem Soc 1958;80:1339–1339.
24. Cao L, Meziani MJ, Sahu S, Sun Y-P. Photoluminescence properties of graphene versus other carbon nanomaterials. Acc Chem Res 2013;46:171–180.
25. Chien C-T, Li S-S, Lai W-J, Yeh Y-C, Chen H-A, Chen IS, Chen L-C, Chen K-H, Nemoto T, Isoda S, Chen M, Fujita T, Eda G, Yamaguchi H, Chhowalla M, Chen C-W. Tunable photoluminescence from graphene oxide. Angew Chem Int Ed Engl 2012;51: 6662–6666.
26. Qian J, Wang D, Cai F-H, Xi W, Peng L, Zhu Z-F, He H, Hu M-L, He S. Observation of multiphoton-induced fluorescence from graphene oxide nanoparticles and applications in in vivo functional bioimaging. Angew Chem Int Ed Engl 2012;51:10570–10575.
27. Li JL, Day D, Gu M. Ultra-low energy threshold for cancer photothermal therapy using transferrin-conjugated gold nanorods. Adv Mater 2008;20:3866–3871.
28. Yang K, Wan J, Zhang S, Zhang Y, Lee S, Liu Z. In vivo pharmacokinetics, long-term biodistribution, and toxicology of PEGylated graphene in mice. ACS Nano 2011;5:516–522.
29. Li JL, Gu M. surface plasmonic gold nanorods for enhanced two-photon microscopic imaging and apoptosis induction of cancer cells. Biomaterials 2010;31:9492–9498.

30. Li JL, Wang L, Liu XY, Zhang ZP, Guo HC, Liu WM, Tang SH. In vitro cancer cell imaging and therapy using transferrin-conjugated gold nanoparticles. Cancer Lett 2009; 274:319–326.
31. Li JL, Liu XY. Fabrication and biofunctionalization of selenium–polypyrrole core–shell nanoparticles for targeting and imaging of cancer cells. J Nanosci Nanotechnol 2008;8:2488–2491.
32. Yang PH, Sun XS, Chiu JF, Sun HZ, He QY. Transferrin-mediated gold nanoparticle cellular uptake. Bioconjugate Chem 2005;16: 494–496.
33. Yang K, Zhang S, Zhang G, Sun X, Lee S, Liu Z. Graphene in mice: Ultrahigh in vivo tumor uptake and efficient photothermal therapy. Nano Lett 2010;10:3318–3323.
34. Tong L, Zhao Y, Huff TB, Hansen MN, Wei A, Cheng J. Gold nanorods mediate tumor cell death by compromising membrane integrity. Adv Mater 2007;19:3136.
35. Hu SH, Chen YW, Hung WT, Chen IW, Chen SY. Quantum-dot-tagged reduced graphene oxide nanocomposites for bright fluorescence bioimaging and photothermal therapy monitored in situ. Adv Mater 2012;24:1748–1754.
36. Akhavan O, Ghaderi E, Aghayee S, Fereydooni Y, Talebi A. The use of a glucose-reduced graphene oxide suspension for photothermal cancer therapy. J Mater Chem 2012;22:13773–13781.
37. Amy RL, Storb R. Selective mitochondrial damage by a ruby laser microbeam—An electron microscopic study. Science 1965;150:756–758.
38. Gu M, Bao HC, Li JL. Cancer-cell microsurgery using nonlinear optical endomicroscopy. J Biomed Opt 2010;15:050502.